Deep-Sea Research II 55 (2008) 1564–1577

Contents lists available at ScienceDirect

Deep-Sea Research II

journal homepage: www.elsevier.com/locate/dsr2

Sinking fluxes of minor and trace elements in the North Pacific Ocean measured during the VERTIGO program

C.H. Lamborg *, K.O. Buesseler, P.J. Lam

Department of Marine Chemistry and Geochemistry, Woods Hole Oceanographic Institution, Woods Hole, MA 02543, USA

ARTICLE INFO

Article history:

Accepted 12 April 2008
Available online 7 May 2008

Keywords:
Mesopelagic zone
Sediment traps
Sinking particles
Organic carbon
Micronutrients
Trace elements

ABSTRACT

As part of the Vertical Transport in the Global Ocean (VERTIGO) program, we collected and analyzed sinking particles using sediment traps at three depths in the oceanic mesopelagic zone and at two biogeochemically contrasting sites (N. Central Pacific at ALOHA; N. Pacific Western Subarctic Gyre at K2). In this paper, we present the results of minor and trace element determinations made on these samples.

Minor and trace elements in the sinking material showed 2 trends in flux with depth: increasing and constant. The sinking particulate phase of some elements (Al, Fe, Mn) was dominated by material of lithogenic origin and exhibited flux that was constant with depth and consistent with eolian dust inputs (ALOHA), or increasing in flux with depth as a result of lateral inputs from a shelf (K2). This shelf-derived material also appears to have been confined to very small particles, whose inherent sinking rates are slow, and residence time within the mesopelagic "twilight zone" would be consequently long. Furthermore, the flux of this material did not change with substantial changes in the rain of biogenic material from the surface (K2), suggesting mechanistic decoupling from the flux of organic carbon and macronutrients.

Micronutrient (Fe, Co, Zn and Cu) fluxes examined in a 1-D mass balance suggest widely differing sources and sinks in the water column as well as impacts from biological uptake and regeneration. For example, total Fe fluxes into and out of the euphotic zone appeared to be dominated by lithogenic material and far exceed biological requirements. The export flux of Fe, however, appeared to be balanced by the eolian input of soluble Fe. For Zn and Cu, the situation is reversed, with atmospheric inputs insufficient to support fluxes, and the cycling therefore dominated by the draw down of an internal pool. For Co, the situation lies in between, with important, but ultimately insufficient atmospheric inputs.

1. Introduction

Compared to macronutrients and biominerals, minor and trace elements are infrequently determined in sinking marine particles (Brewer et al., 1980; Martin and Knauer, 1983; Jickells et al., 1984; Kremling and Streu, 1993; Kuss and Kremling, 1999; Nameroff et al., 2002; Ho et al., 2003; Pohl et al., 2004, 2006; Stanley et al., 2004; Frew et al., 2006). This is especially true for mid-water depths, within the mesopelagic or so-called "twilight zone" of the oceanic water column. This is unfortunate as this depth region is where bacterial and zooplankton respiration and physical and chemical forcings attenuate much of the downward particle flux exiting the euphotic zone (Volk and Hoffert, 1985; Ducklow et al., 2001). As the mesopelagic zone overlaps in some places with the deep winter mixed layer, the remineralization of sinking particles in this region can result in resupply of micronutrient elements as well as those that may have significant anthropogenic inputs to the euphotic zone over an annual cycle. As many parts of the ocean are limited in primary production by one or perhaps more micronutrient species (e.g., Fe, Co, Zn and Cd; Morel et al., 2004), studies of the cycling of minor and trace elements within the mesopelagic zone are an important component in understanding marine biogeochemistry and ecology as well as the marine chemistry of trace elements.

We present here the results of minor and trace element determinations on sinking particles collected by sediment traps, as part of the Vertical Transport in the Global Ocean program (VERTIGO; Buesseler, Valdes, Siegel, Steinberg, PI's). The wider goal of this project was to study the inner workings of the biological pump in the marine mesopelagic zone through the collaborative, inter-disciplinary examination of the biology, chemistry and physics of two contrasting oceanic provinces (see Buesseler et al., 2008). Much of the motivation for such work is to gain a greater understanding of the ocean's ability to sequester organic carbon. However, this effort benefits from studying additional components of the sinking flux, including biomineral/ballasting phases such as opal, calcium carbonate, lithogenic particles and biological rates of processing,

* Corresponding author. Tel.: +1 508 289 2556.
E-mail address: clamborg@whoi.edu (C.H. Lamborg).

0967-0645/$ - see front matter © 2008 Elsevier Ltd. All rights reserved.
doi:10.1016/j.dsr2.2008.04.012

and the cycling of tracer and micronutrient elements like those presented here.

2. Study sites

The two study sites for the VERTIGO program were located in the North Pacific Ocean, at stations that represent two contrasting biogeochemical systems. The first station occupied was ALOHA, located just north of the Hawaiian island of Oahu (22.75°N 158°W; Fig. 1) and the primary study location for the Hawaiian Ocean Time-series (HOT) program (http://hahana.soest.hawaii.edu/hot). This site is located in the oligotrophic open-ocean gyre of the subtropical North Pacific, and is characterized by relatively little seasonal variation in physical and biological behavior, and a producer community dominated by relatively small and generally non-mineral forming cells (e.g., Karl and Michaels, 1996). Our ALOHA occupation took place from June 22 to July 8, 2004.

The second site occupied, K2 (47°N 160°E; Fig. 1), was part of a Japan Agency for Marine-Earth Science and Technology (JAMSTEC) time-series program and our field work there was conducted between July 24 and August 16, 2005. In contrast to ALOHA, K2 is an HNLC, Fe-limited region that undergoes large seasonal fluctuations in production and community structure (Honda et al., 2002; Tsuda et al., 2003). At the time of our occupation, and as is typical in late summer in this location, the primary producer community was dominated by diatoms, and large grazing zooplankton were also found (M.W. Silver, pers. comm.; Steinberg et al., 2008). At K2, dissolved oxygen drops to very low ($<50\,\mu M$) levels below the halo/pycnocline and remains low through most of the mesopelagic zone. This appears to be a combination of local oxygen consumption and advection from the Bering Sea shelf (e.g., Reid, 1997; Andreev and Kusakabe, 2001). Station locations as well as modeled dust fluxes for the North Pacific are shown in Fig. 1. Additional description of both sites can be found elsewhere (e.g., Buesseler et al., 2007b, 2008).

3. Methods

3.1. Trapping systems

This report contains data from two different types of sediment trap systems. These included a surface tethered system ("Clap Trap") similar to that used during JGOFS and at the HOT and BATS time-series, as well as neutrally buoyant sediment traps (NBSTs; Buesseler et al., 2000; Valdes and Price, 2000). It is hypothesized that the NBSTs should yield more reliable flux values than the tethered traps, because as free vehicles they experience very little hydrodynamic slip, and therefore should be free of over- and undercollection and particle sorting biases due to hydrodynamics that are known to affect tethered or moored traps (e.g., Buesseler et al., 2007a).

The details of the sediment trap systems and their use during VERTIGO are included in companion papers (Lamborg et al., 2008; Buesseler et al., 2008). In brief, both tethered (Clap Traps) and neutrally bouyant (NBST) traps were twice deployed at three depths (150, 300 and 500 m) on each cruise for 3–5 days depending on depth. Both kinds of traps consisted of 5 (NBST) or 10 (Clap) polycarbonate cylinders, which were deployed containing filtered seawater and a 500 mL bottom layer of buffered, trace metal-clean brine that was poisoned/preserved with either formalin or $HgCl_2$ (Lee et al., 1992) to retard bacterial degradation of the collected particles. The brine was formed by freeze-concentrating filtered, low-metal, Sargasso Sea water, avoiding the need for adding metal-contributing salts. The buffering was provided by a borate solution (pH = 8.2), made with high-purity boric acid (Puratronic®, Alfa Aesar) and NaOH, and nominally increased the alkalinity of the brine to twice that of unamended brine. The Clap Trap arrays also carried a blank process tube, which was identical in all respects to the samples, but was deployed closed.

3.2. Recovery and processing

After recovery of each system/device, the two sample tubes with Hg-poisoning were combined, as were the two sample tubes preserved with formalin, after passing the water/particle mixture through a 350 μm screen to remove zooplankton swimmers. The combined tube material was then wet split at sea into eight equal portions. Each of these splits were filtered onto different types of filter media to allow for a variety of elemental and pigment determinations, including particulate organic carbon (POC), particulate inorganic carbon (PIC) and biogenic silica (bSi). Combining tubes and splitting the pooled samples allowed direct comparison between a variety of parameters without introducing tube-to-tube variability (Lamborg et al., 2008). Minor and trace element determinations were made on the sample splits used for

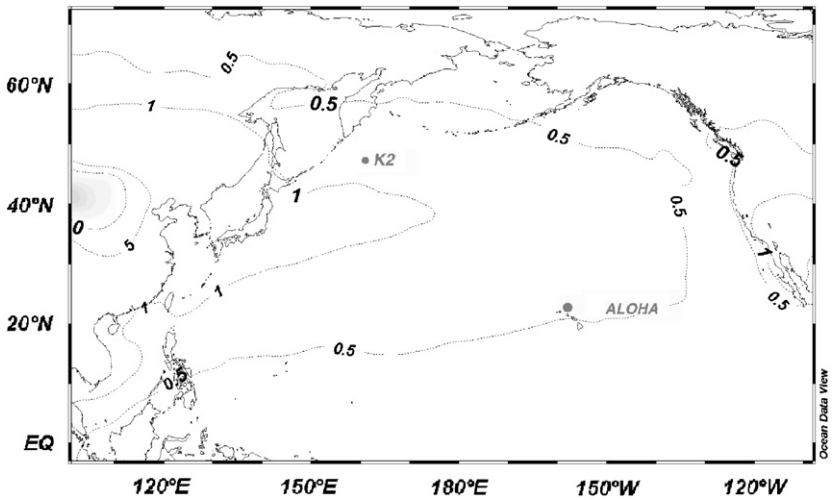

Fig. 1. The locations of the two sites occupied during the VERTIGO program as well as contours of aeolian dust deposition ($g\,m^{-2}\,y^{-1}$). The dust flux estimates were presented in Mahowald et al. (2005), and the figure prepared with values generously provided by N. Mahowald.

mass determination that had been filtered onto acid-washed, pre-weighed, 1.0 μm pore sized, 25 mm Nuclepore membranes. Filtrates were not analyzed for trace elements. Following the filtering, the membranes were rinsed with a small amount of pH 8.2, borate-buffered 18 MΩ cm^{-1} water. Upon return to the lab following collection, the samples were desiccated and weighed multiple times to a constant weight. During weighing, the filters were handled cleanly so that element analyses could be performed on the same filters.

All components of the sediment traps as well as the plasticware used in handling/processing were rigorously acid-cleaned, including the tubes, swimmer screens, collection bottles, minor/trace element split bottles, filtering rigs and forceps. Furthermore, much of the sample handling, such as splitting and filtering, was conducted under a HEPA filtering laminar flow bench.

3.3. Elemental analysis

Minor and trace elements were determined by Magnetic Sector Inductively Coupled Plasma Mass Spectrometry (ICP-MS). The methods used here were similar to those used during preliminary NBST development (Stanley et al., 2004). In brief, aliquots were cut from the whole filter using ceramic scissors and the sample fraction determined gravimetrically. The aliquots were then digested in a hot block (120 °C) for >4 h in small sealed Teflon vials (Savillex). The digestion solution was a 5 mL 4:1 mixture of concentrated trace metal grade HNO_3 and HF. Some samples were also pre-digested with 0.2 mL of concentrated NH_4OH to aid in filter dissolution, but results suggested that incomplete digestion of the filter matrix made little difference to the results (see Fig. 2). Following cooling of the sample, 0.1 mL of saturated boric acid solution was added to aid in dissolution of CaF_2 (e.g., Collier, 1991). The concentrated samples were held until analysis in acid-washed low-density polyethylene vials. Prior to analysis, the concentrated digest was quantitatively diluted by ca. 20 × with a 5% acid solution (4:1 HNO_3:HF) also spiked to ca. 0.5 ppm with ^{115}In. The In-spiked diluent was made in bulk so that all samples analyzed during a single day would be diluted with a solution containing identical In concentrations. A similar digestion approach was recently compared to a borate fusion method, and found to agree well for most elements (Huang et al., 2007).

The diluted samples were analyzed on a Thermo Electron Finnigan Element 2, outfitted with an Aridus desolvating nebulizer and ASX-100 autosampler (both CETAC), with sample take-up rates at 0.1 mL min^{-1}. ^{114}Cd, ^{115}In, ^{137}Ba and ^{208}Pb were measured in low resolution ($\Delta = 300$) with 20 scans while ^{23}Na, ^{25}Mg, ^{27}Al, ^{31}P, ^{44}Ca, ^{45}Sc, ^{47}Ti, ^{51}V, ^{55}Mn, ^{56}Fe, ^{59}Co, ^{60}Ni, ^{63}Cu, ^{66}Zn and ^{88}Sr were measured in medium resolution ($\Delta = 4000$) for 5 scans. No results from Cd, Pb, Ti and Ni are shown as they appeared to be unreliable due to large (relative to the sample signals; Cd, Pb) and/or variable process blanks (Ti, Ni). Ni was likely unreliable due to the use of Ni skimming cones in the ICP-MS, but the cause of the occasional spurious Ti results is unknown.

Two different SRMs were processed and analyzed by ICP-MS as well (NRC HISS-1 and MESS-3). Results agreed with certified values within 10% in most cases (Table 1).

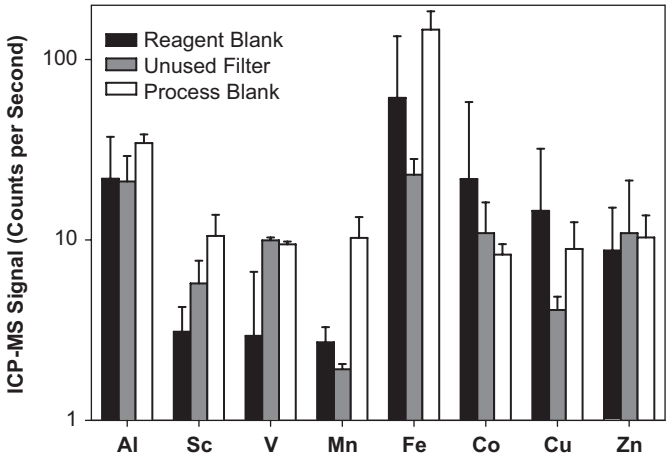

Fig. 2. Analysis of sources of blank signal to ICP-MS analyses. In most cases, the reagents (digestion acids, borate, lab water used for dilution) represent the majority of the signal. These signals are not corrected for residual seawater using the Na signal, which likely explains the large Ca process blank value.

3.4. Process blanks

As noted, the covered tube on board the Clap Trap array was used as a process blank, and subjected to all the same processing protocols as the samples. The blank "fluxes" are included in Table 2 for comparison to the samples and are calculated by dividing the average blank value for each parameter by a nominal deployment time of 4 days. However, blank correction was made to each trap system on a mass, and not flux, basis. It should be noted that the use of a process blank is rarely seen in sediment trapping programs. While most samples were well above their respective detection limits, the process blanks often represented non-trivial fractions of the sample, as shown in Table 2. Sodium found in the sediment trap material was assumed to be the result of retention of seawater salt, and was therefore used to correct element fluxes for this artifact. None of the minor and trace elements reported here required a significant seawater correction.

A breakdown of the contribution to the minor and trace element value of the blank is shown in Fig. 2. In most cases, the reagents were the largest contributor to the ICP-MS signal, while the filter material typically added little. In only some cases, for example Mn and to a lesser extent Fe, the process blank was higher than either the filter or reagent blank, representing contributions from filter/tube handling and processing. It is unclear why these two elements should be more susceptible to handling blanks than the others, but still represent relatively small blank values when compared to samples.

3.5. In-trap solubilization experiments

Although the traps were poisoned/preserved/buffered, degradation of collected particles can occur before recovery and processing of the samples, resulting in flux estimates that are biased low (e.g., Antia, 2005). To examine whether such an effect was significant in our deployments, we selected two of the poisoned tubes on the Clap Traps to be combined and used the splits as individual time points in aging experiments. The splits were held in the dark and at temperatures representative of the depths from which they came (i.e., 25, 15 and 5 °C for 150, 300 and 500 m at ALOHA and 4 °C at K2), and were observed to experience little pH change for the duration of the experiment (<0.2 pH units). No attempt was made to control the redox state of the samples (the container lids were left loose to avoid anoxia), which could have resulted in increased oxygen concentrations in the two deepest samples from K2 (the other samples were collected under conditions of relative oxygen abundance). The splits were sacrificed at specific times (1, 2, 3 and 5 days after collection) as with regular samples. Only the particle phase was analyzed for minor and trace element concentrations. The amount of flux that could have been lost to solubilization was determined by fitting

Table 1
Summary of standard reference material analyses for minor/trace elements reported for trap samples

Standard reference material	N	Al	Sc	V	Mn	Fe	Co	Cu	Zn
NRC HISS-1	11	109±7	Undefined	102±17	98±19	107±17	114±30	96±4	107±26
NRC MESS-3	14	101±17	Undefined	107±17	105±13	110±16	106±20	95±12	81±20

Values are average and standard deviation percents of certified value. Sample sizes were similar to trap sample sizes (a few mg), and are smaller than those recommend by the National Research Council of Canada to ensure homogeneity (250 mg).

the changes in particulate metal concentrations with first-order exponential decay curves, and using the apparent reaction rate constants to determine the "true" flux according to

$$F = \frac{kx_t}{1 - e^{-kt}}$$

where F is the flux of an element falling into the trap, k is the fitted decay constant, x_t is the amount of the element found in the trap at the end of the deployment and t is the deployment time. The results of these experiments are discussed in greater detail in a companion paper (Lamborg et al., 2008), but are summarized here with respect to their impact on minor and trace element fluxes.

None of the K2 aging experiments yielded discernible loss of particulate minor and trace elements over 5 days. For the ALOHA samples, only one sample (the 500 m Clap Trap during the first deployment) exhibited a significant loss of trace metals, and was confined to Fe and Mn. The apparent correction for flux suggested by the aging experiment results for that sample were 24±7% for Fe and 47±14% for Mn. Though significant in these cases, the evidence for in-trap solubilization was isolated and not systematic at ALOHA, so no correction to the apparent flux for Fe and Mn was made for that sample.

The lack of an in-trap solubilization signal is perhaps not surprising, as these deployments were relatively short (<5 days), as opposed to multi-month, moored trap studies using automated collectors (e.g., Antia, 2005).

3.6. XRF analysis of trap material

X-ray Fluorescence (XRF) data were collected at the synchrotron XRF microprobe at beamline 10.3.2 of the Advanced Light Source, Lawrence Berkeley National Laboratory, in December 2005 and May 2006. Zn and Fe data were collected at an incident beam energy of 10 keV; Mn data were collected below the Fe K-edge at 6588 eV to prevent leakage into the Mn channel from Fe; Si data were collected at 4038 eV with the sample bathed in an He environment. All other elements were collected with the sample in air. Aluminum is not detectable using this particular beamline. The pixel size was 5 μm and the dwell time per pixel was 100 ms. Blank filter values were subtracted from the samples, and all elements were standardized using NIST thin-film XRF standards.

4. Results and discussion

4.1. Fluxes of mass and biogenic material at both sites

The vertical profiles of particle flux for both sites are shown in Figs. 3 and 4. The fluxes of mass and major biogenic components are discussed at length elsewhere (Buesseler et al., 2007b; Lamborg et al., 2008); however, the salient points are highlighted in this section and figures for the flux profiles of mass and POC are included in Figs. 3 and 4 and Table 2 to provide context for interpreting the trace element data. The two different trapping systems yielded similar results for minor and trace element fluxes. This is in contrast to many components of biogenic flux, where the Clap Traps appeared significantly lower during the first deployment at K2 (Lamborg et al., 2008). To be consistent with our discussions of major phases elsewhere, we focus most of our discussion on NBST data in this report, but the Clap data are included in the tables and some of the figures for comparison.

The composition of the sinking particles at the two sites was decidedly different. The sinking particles at ALOHA were composed of about 40–60% particulate organic matter (POM; POC x 2.2; Klaas and Archer, 2002) by mass, with PIC, bSi and lithogenic material making up the rest (in that order of importance). In contrast, the K2 material caught by the traps was about 80% bSi, with most of the remaining mass made up of POM, and minor contributions from PIC and lithogenics.

The fluxes of the major biogenic material components (POC, N, P, bSi, PIC) all appeared to decrease with depth. The effect was much less at K2 than at ALOHA, and this may be the result of a number of factors, including inherently less degradable, larger and therefore faster sinking particles as well as colder temperatures at K2 (Buesseler et al., 2007b). In addition to much higher transfer efficiencies through the mesopelagic zone at K2, the PIC/POC ratio was also lower, making the biological pump at this location more effective at sequestering CO_2 (e.g., Dymond and Lyle, 1985; Frankignoulle et al., 1994).

The fluxes of all material at ALOHA were nearly constant between the deployments, as might be expected from a system that experiences relatively little seasonal variability, and consistent with our simultaneous observations of relatively constant chlorophyll concentrations, production rates and zooplankton biomass (Buesseler et al., 2008; Steinberg et al., 2008).

Unlike ALOHA, the fluxes of most major particle components at K2 were much higher during the first deployment than in the second. For example, fluxes of mass and POC shown here, as well as N, P, PIC and bSi all dropped by factors of 2–5 between deployments (Lamborg et al., 2008).

4.2. Fluxes of minor and trace elements at both sites

The fluxes of minor and trace elements are shown in Table 2 and Figs. 3 and 4. The elements showed either increasing (Fe, Al, Mn and Sc at K2) or approximately constant fluxes with depth. The magnitudes of element fluxes were similar at both sites, except for much higher fluxes of Zn and V at K2 and cobalt at ALOHA. These trends, their possible causes and biogeochemical context are discussed in separate sections below.

4.2.1. Flux of dust-derived lithogenic material at ALOHA and K2

If we assume that all Al sinking through the mesopelagic is from lithogenic material and that this material is 7.96% Al by weight (Wedepohl, 1995), the measured flux at ALOHA (~0.3 mg Al m^{-2} d^{-1}) translates into 4 mg lithogenics m^{-2} d^{-1}. This value is consistent with an estimate of dust input to the region based on aerosol measurements and estimates of dry deposition velocity (1.2–12 mg dust m^{-2} d^{-1}; e.g., Duce et al., 1991; Zieman et al.,

Table 2
Flux summaries for ALOHA and K2

Site/deployment	Device	Depth (m)	Mass ($mg\,m^{-2}\,d^{-1}$)	POC ($mmole\,m^{-2}\,d^{-1}$)	Al ($\mu g\,m^{-2}\,d^{-1}$)	Sc ($ng\,m^{-2}\,d^{-1}$)	V ($\mu g\,m^{-2}\,d^{-1}$)	Mn ($\mu g\,m^{-2}\,d^{-1}$)	Fe ($\mu g\,m^{-2}\,d^{-1}$)	Co ($\mu g\,m^{-2}\,d^{-1}$)	Cu ($\mu g\,m^{-2}\,d^{-1}$)	Zn ($\mu g\,m^{-2}\,d^{-1}$)
(a) for ALOHA												
ALOHA, 1st	NBST 13	150	n/a	n/a	n/a	n/a	n/a	n/a	n/a	n/a	n/a	n/a
ALOHA, 1st	NBST 15	150	69±9	1.53±0.25	466±70	163±n/a	<dl	2.8±1.3	322±160	3.03±2.56	2.56±1.21	40.8±n/a
ALOHA, 1st	NBST 17	150	51±6	1.39±0.43	280±105	69±32	<dl	1.0±0.1	140±67	2.72±0.03	1.05±0.18	<dl
ALOHA, 1st	NBST 14	300	30±14	0.61±0.20	235±211	64±n/a	<dl	5.9±4.0	220±n/a	4.94±0.00	1.32±0.31	<dl
ALOHA, 1st	NBST 16	300	29±3	0.54±0.03	451±229	69±32	<dl	9.2±4.2	228±n/a	3.36±0.08	1.64±0.43	<dl
ALOHA, 1st	NBST 11	500	13±8	0.37±0.05	158±71	52±n/a	<dl	2.9±1.8	137±79	3.70±0.10	0.93±0.66	<dl
ALOHA, 1st	NBST 12	500	17±3	0.29±0.01	230±167	57±15	<dl	3.4±1.2	145±91	4.13±0.56	2.38±n/a	<dl
ALOHA, 1st	CLAP TRAP	150	73±3	n/a	288±n/a	59±n/a	<dl	4.8±n/a	337±n/a	3.26±n/a	0.64±n/a	<dl
ALOHA, 1st	CLAP TRAP	300	37±5	0.65±0.02	457±96	81±50	<dl	11.3±4.1	376±91	4.01±0.97	1.36±0.53	<dl
ALOHA, 1st	CLAP TRAP	500	29±2	0.57±0.09	372±147	85±8	<dl	9.4±2.2	290±28	4.06±0.10	1.82±1.36	10.0±0.5
ALOHA, 2nd	NBST 13	150	61±5	1.28±0.08	191±26	127±n/a	<dl	1.5±0.5	149±54	0.53±n/a	0.73±n/a	<dl
ALOHA, 2nd	NBST 15	150	50±3	1.35±0.02	139±n/a	<dl	<dl	<dl	124±n/a	4.96±0.09	0.77±n/a	9.9±n/a
ALOHA, 2nd	NBST 17	150	80±27	1.86±0.71	132±99	<dl	<dl	1.7±n/a	251±102	5.11±n/a	0.76±0.53	13.1±0.7
ALOHA, 2nd	NBST 14	300	29±3	0.65±0.16	110±15	<dl	<dl	1.9±0.4	100±3	5.02±0.07	0.52±0.31	8.0±n/a
ALOHA, 2nd	NBST 16	300	29±2	0.40±0.07	139±7	<dl	<dl	2.3±0.3	133±1	4.48±0.57	0.64±0.11	<dl
ALOHA, 2nd	NBST 11	500	18±1	0.31±0.08	112±26	<dl	<dl	2.6±0.2	95±23	5.05±0.06	0.97±0.19	<dl
ALOHA, 2nd	NBST 12	500	17±9	n/a	279±n/a	51±n/a	<dl	4.0±n/a	188±n/a	<dl	1.57±n/a	<dl
ALOHA, 2nd	CLAP TRAP	150	65±8	1.11±0.30	152±127	70±n/a	<dl	3.6±n/a	243±n/a	2.58±0.68	1.23±1.11	15.8±n/a
ALOHA, 2nd	CLAP TRAP	300	43±6	0.71±0.07	364±56	78±9	<dl	7.3±1.3	264±20	<dl	1.32±0.21	12.1±n/a
ALOHA, 2nd	CLAP TRAP	500	25±3	0.39±0.02	334±53	66±0	<dl	7.0±0.3	236±16	<dl	1.16±n/a	<dl
ALOHA	Blk[a]	150	8±2	0.11±0.04	12±2	17±28	0.3±0.1	0.6±0.5	24±15	0.0±0.2	0.0±0.2	0.2±0.6
(b) for K2												
K2, 1st	NBST 13	150	963±146	4.88±n/a	n/a	n/a	n/a	n/a	n/a	n/a	n/a	n/a
K2, 1st	NBST 15	150	896±53	4.89±n/a	267±77	149±n/a	2.77±0.50	6.29±1.86	136±51	0.20±0.04	7.41±5.93	286±37
K2, 1st	NBST 17	150	959±123	5.68±n/a	188±55	119±n/a	3.29±1.67	4.41±1.02	92±30	2.06±n/a	5.31±3.10	529±186
K2, 1st	NBST 14	300	1102±79	4.11±n/a	490±180	181±88	3.08±1.41	14.14±4.36	309±103	0.50±n/a	5.11±1.02	453±99
K2, 1st	NBST 16	300	924±120	3.67±n/a	555±44	231±61	3.72±0.05	19.29±0.53	386±28	0.25±0.10	12.07±3.49	327±1
K2, 1st	NBST 11	500	n/a	n/a	n/a	n/a	n/a	n/a	n/a	n/a	n/a	n/a
K2, 1st	NBST 12	500	490±144	2.39±n/a	612±318	177±88	3.07±1.39	21.40±11.10	504±177	0.36±0.15	5.56±1.46	380±179
K2, 1st	CLAP TRAP	150	525±170	3.64±n/a	378±136	175±139	1.83±0.92	10.61±6.01	256±205	1.02±1.14	3.00±1.24	366±150
K2, 1st	CLAP TRAP	300	402±113	2.27±n/a	817±809	238±n/a	2.02±0.81	12.57±7.70	313±265	0.53±0.55	5.36±3.26	397±392
K2, 1st	CLAP TRAP	500	421±109	2.69±n/a	595±155	239±35	2.84±0.52	20.82±4.03	419±55	0.59±0.26	8.16±2.33	387±320
K2, 2nd	NBST 13	150	227±53	2.06±n/a	271±n/a	147±n/a	1.40±n/a	8.89±n/a	236±n/a	n/a±0.00	3.96±n/a	176±n/a
K2, 2nd	NBST 15	150	290±20	1.91±n/a	228±32	152±n/a	1.41±0.15	5.58±0.92	77±9	0.16±n/a	2.28±0.24	99±1
K2, 2nd	NBST 17	150	260±34	1.81±n/a	207±96	152±82	1.78±0.21	5.47±2.39	128±87	0.61±n/a	6.20±1.86	144±9
K2, 2nd	NBST 14	300	222±23	1.21±n/a	472±17	162±55	1.88±0.09	16.23±4.55	376±169	0.22±0.11	3.60±0.28	112±18
K2, 2nd	NBST 16	300	223±69	1.51±n/a	544±30	174±45	2.34±0.24	15.49±1.25	288±7	0.17±0.02	5.42±1.29	115±20
K2, 2nd	NBST 11	500	167±26	1.01±n/a	516±94	189±89	1.96±0.34	19.42±2.86	342±47	0.21±0.03	4.35±1.20	111±7
K2, 2nd	NBST 12	500	219±32	1.12±n/a	446±154	178±41	1.88±0.34	14.94±4.40	252±97	0.60±0.33	7.04±5.09	170±72
K2, 2nd	CLAP TRAP	150	285±54	1.92±n/a	308±145	146±n/a	1.78±0.29	8.61±2.26	396±88	0.54±n/a	6.68±3.35	181±34
K2, 2nd	CLAP TRAP	300	296±22	1.82±n/a	772±38	215±33	3.32±0.06	19.94±2.96	548±76	0.30±0.02	7.15±0.47	215±61
K2, 2nd	CLAP TRAP	500	204±80	1.12±n/a	883±115	265±51	3.36±0.09	28.50±3.02	644±23	0.40±0.00	7.07±2.07	217±103
K2	Blk[a]	All	28±14	0.34±0.04	0±46	17±60	0.14±0.22	0.00±0.57	88±88	0.06±0.06	0.1±0.1	5±5

n/a is not available. <dl is below detection (nominally 3 s of blank tubes).

[a] The blank ("Blk") values are taken from the covered, process blank tubes on board the Clap Traps ($N = 6$). The magnitude of the blank is divided by the nominal deployment time of 4 days to get a blank "flux" to compare the measured sample fluxes. The sample values have been blank corrected.

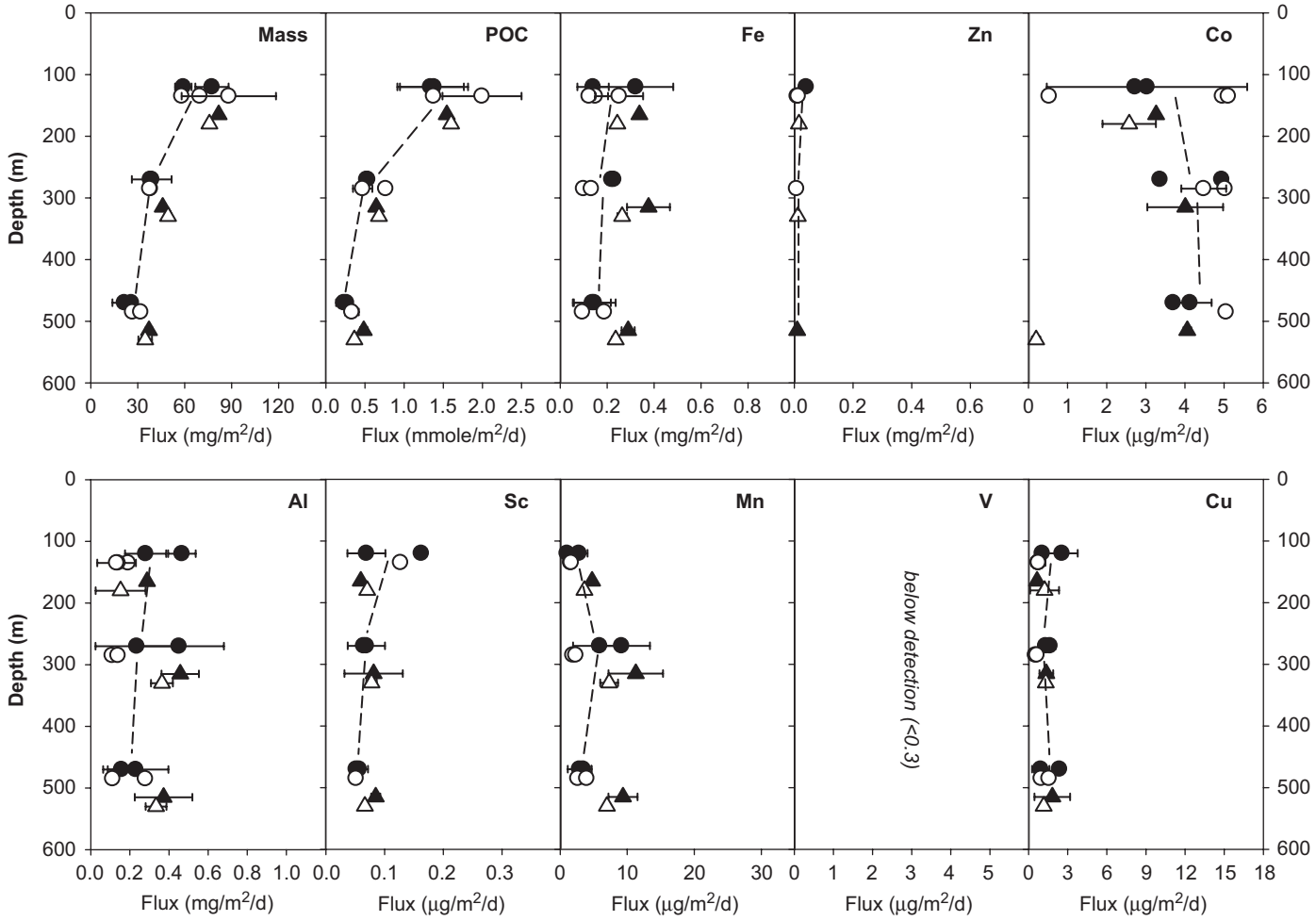

Fig. 3. Average flux of mass, POC, minor and trace elements at ALOHA. The mass, POC and other major component results are discussed in a companion paper (Lamborg et al., 2008), and shown here for comparison. Circles—NBST; triangles—clap traps; first deployment—black; second deployment—white. Error bars are 1SD.

1995; ca. 2 mg dust $m^{-2} d^{-1}$, Jickells et al., 2005) but higher than, though within an order of magnitude of estimates based on dissolved Al concentrations in regional surface waters (0.3–1.6 mg dust $m^{-2} d^{-1}$; Measures and Vink, 2000; Measures et al., 2005). It should be noted that the dissolved Al approach to estimating dust fluxes (the MADCOW model; Measures and Vink, 2000) integrates over the residence time of dissolved Al (3–6.5 years), whereas our trap measurements integrate over a much shorter time. Thus, some discrepancy between these two measurements might be expected due to some amount of temporal variability. Furthermore, elements whose inputs to the ocean are thought to be dominated by dust (Fe, Mn and Sc), showed correlations with Al at ALOHA and in proportions similar to those of crustal materials (Fig. 5). The flux of Al and the other apparently dust-derived components at ALOHA were essentially constant with depth, suggesting the supply and removal of dust-derived lithogenic material was in steady state during our sampling.

As with ALOHA, the 150 m Al fluxes at K2 (~0.2 mg Al $m^{-2} d^{-1}$ and therefore 2.5 mg lithogenics $m^{-2} d^{-1}$) were consistent with atmospheric dust input as a primary source (0.2–1.64 mg dust $m^{-2} d^{-1}$; Measures et al., 2005). Though Asian dust plumes sometimes move over the region, our flux measurements suggest there was not a large amount of dust deposition to the region during our occupations. This was confirmed by the satellite aerosol index product available from OMI (toms.gsfc.nasa.gov/aerosols/) for the weeks leading to our occupation. Recent modeling suggests that dust loadings are generally not as high in this location as previously suggested (Mahowald et al., 2005; Jickells et al., 2005).

4.2.2. *Increasing fluxes of crustal tracers at K2*

Though the fluxes of Al and other crustal components at 150 m were consistent with dust inputs at the surface, their fluxes increased with depth at K2 (Fig. 4). In addition, the flux of Mn at 300 and 500 m was much greater than would be expected if dust were its primary source, as indicated by Mn/Al ratios that are elevated above crustal values (Fig. 6). The super-crustal ratio of Mn to Al in trap samples, along with the trend of increasing fluxes of Al, Mn and Fe with depth, the maxima in suspended particle Fe and Mn between 135 and 185 m (Lam and Bishop, 2008), and an enhancement of ^{228}Ra over equilibrium (M. Charette, pers. comm.) all suggest that a lateral plume from a nearby continental shelf is responsible for a substantial amount of the flux of lithogenic elements at K2, particularly below 150 m (ca. 50% of flux at 300 and 500 m). Nishioka et al. (2007) also invoked a margin source to explain high subsurface Fe at the nearby Station KNOT. The enhancement of the flux of Mn relative to Al is made possible by the shelf source, as reducing conditions in shelf sediments are able to mobilize Mn that is then slow to re-oxidize and can be carried long distances (e.g., Bishop and Fleisher, 1987; Johnson et al., 1992). This plume of shelf-derived particulate Al, Fe and Mn is likely losing particles to gravitational settling and repackaging as it is being advected laterally. Alternatively in the case of Mn, the

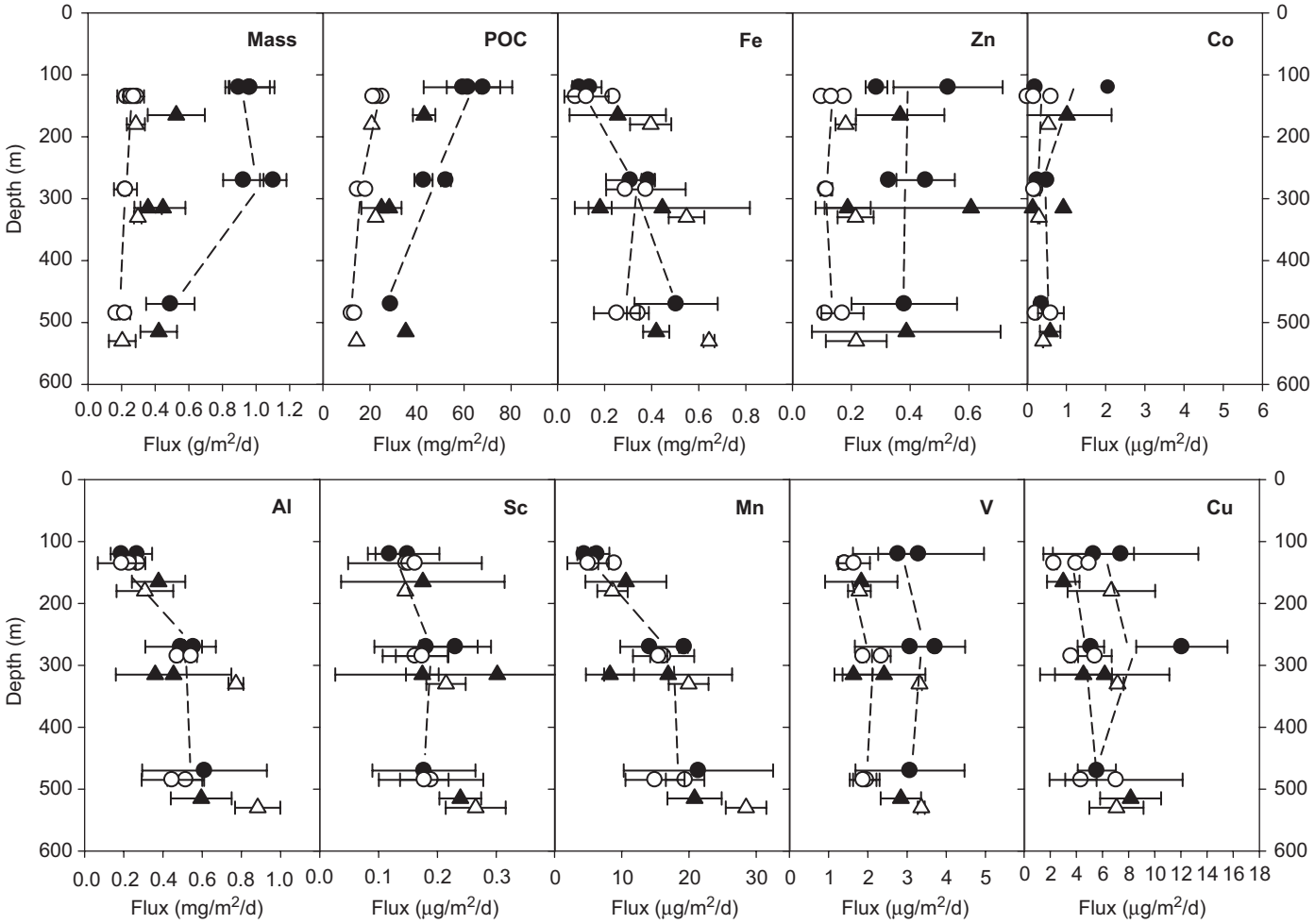

Fig. 4. Average fluxes at K2. Plotting conventions same as Fig. 2.

advecting plume is in the form of dissolved Mn(II) which oxidizes and enriches particulate Mn during transport (e.g., Moffett and Ho, 1996). As an example of the effect of the plume, only about 0.6% d^{-1} of the plume must sink into the traps to account for the Mn enhancements with depth (flux enhancement is ~15 μg m^{-2} d^{-1} between 150 and 300; with an average plume concentration of ~16 μg m^{-3}, plume inventory is ~2400 μg m^{-2} is this layer; Lam and Bishop, 2008). This relatively slow rate is consistent with long distance dispersion of such a plume from a remote shelf. A similar calculation can be made for the Fe flux enhancement as well (average plume concentration of total Fe of about 110 μg m^{-3}; plume inventory of ~16,500 μg m^{-2}; flux enhancement below 150 m of ~200 μg m^{-2} d^{-1}), leading to a calculated plume "decay" rate of 1.2% d^{-1}. Although this is still a relatively slow rate of decay, the difference between the apparent lifetimes of Mn and Fe suggests they are present in the plume in different forms. Since much of the Mn present in the plume was probably authigenically precipitated during transport, it may exist in the plume as very small particles, whereas Fe would be found on slightly larger, resuspended sediment particles that would have a shorter residence time in the water column. Examination of the trap samples by XRF microprobe supports the idea of Fe and Mn entering the traps as distinct, discrete particles, with the distributions of these two metals appearing in highly concentrated, micron-scale particles that tended not to co-locate with each other (Fig. 7). Only acid-leachable (not total) particulate Al data are available from MULVFS (Bishop, pers. comm.), but a similar calculation (average plume concentration of acid-leachable Al of ~54 μg m^{-3}; plume inventory of ~8100 μg m^{-2}; flux enhancement below 150 m of ~300 μg m^{-2} d^{-1}) leads to an upper limit for the calculated plume decay rate of 3.7% d^{-1}, consistent with Al being in larger, resuspended sediment particles bearing Fe.

4.2.3. *Decoupling of biogenic and lithogenic fluxes*

Of particular interest is that the flux of lithogenic-associated material did not change in concert with the biogenic phases. For example, at ALOHA, the flux of elements such as Al, Fe and Mn did not change vertically despite rapid attenuation of biogenic material (Fig. 3), and at K2, the fluxes did not change between deployments despite large decreases in biogenic flux (Fig. 4).

The systematics of the lithogenic elements is in contrast to trace elements such as Zn, whose flux patterns mirrored those of the major phases. These behavior differences are consistent with their XRF spatial distributions, with Zn more evenly distributed (as is Si) in contrast to the heterogeneous distributions of Fe and Mn (Fig. 7). The dramatic decrease in particle flux from deployments one to two at K2 can be seen in the decreased intensities of the Si and Zn XRF maps, while Fe remains similar in both deployments (Fig. 7). Taken together, this information suggests that such small particles are not scavenged very effectively, and likely enter the traps as discrete particles. While sinking aggregates may act as "nets" for other particle types such as $CaCO_3$ coccoliths (e.g., Passow and De La Rocha, 2006), it appears that this may not be true for small lithogenics.

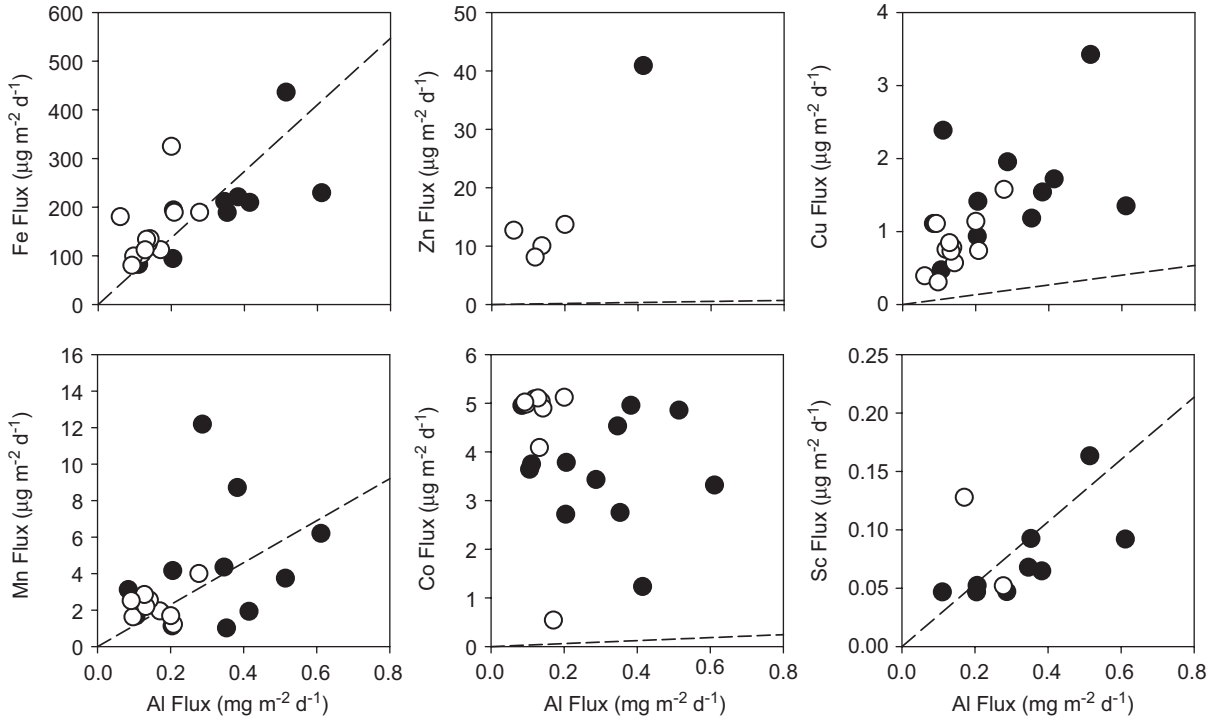

Fig. 5. Correlations of minor and trace elements with Al in sediment trap samples at ALOHA. NBST data only, with first deployment black and second in white. Individual samples (rather than averages, as in Figs. 2 and 3) are shown to illustrate variability. Crustal ratios are indicated by the dashed line.

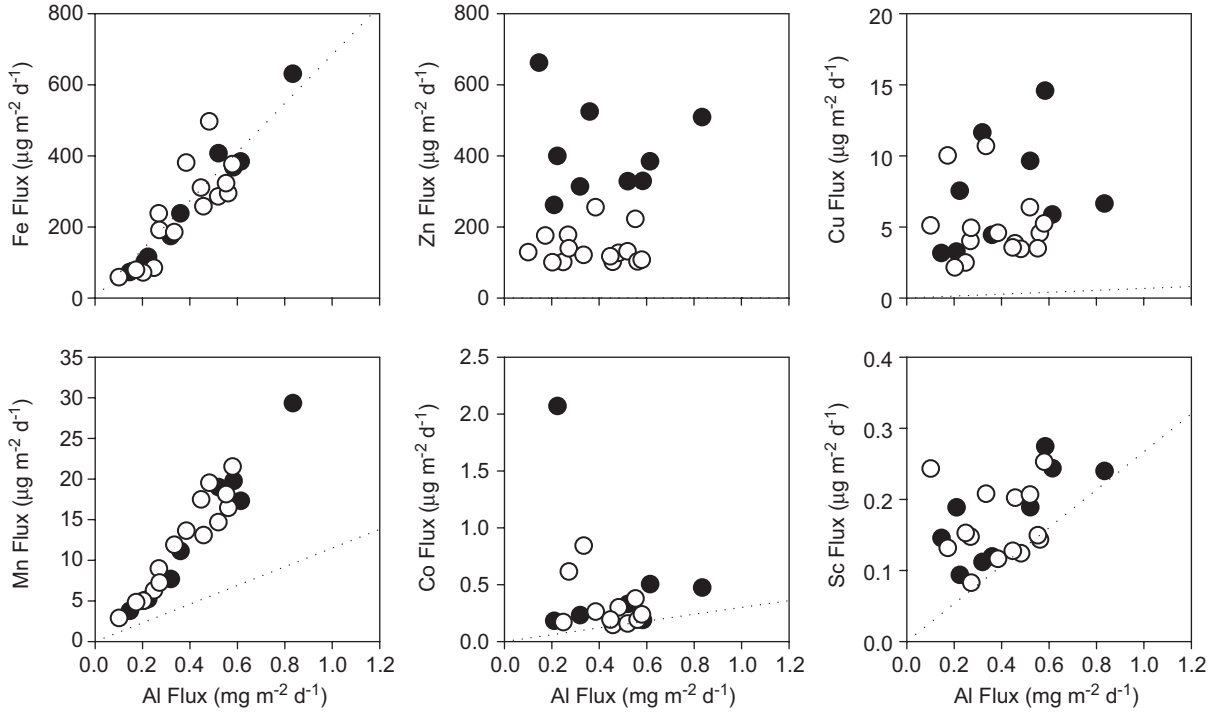

Fig. 6. Correlations of minor and trace elements with Al in sediment traps at K2. NBST data only, with first deployment black and second in white. Crustal ratios indicated by the dashed line.

This decoupling can also be demonstrated by determining the remineralization length scale of the metals measured. We did this by calculating the exponent (b) for a power law ($\text{Flux} = \text{Flux}_{100} * (z/100)^{-b}$; Martin et al., 1987) through non-linear curve fitting. As can be seen in Table 3, the b values for Fe, Al and Mn are much smaller than for the biogenic components (taken from Lamborg et al., 2008), indicating less flux attenuation with depth. A similar observation was made for Fe in the South Pacific during the FeCycle experiment (e.g., Croot et al., 2007; Frew et al., 2006), where Fe:C ratios were observed to increase in sinking particles with depth. Such difference in length scales is one of the factors that tends to maintain the ferricline at

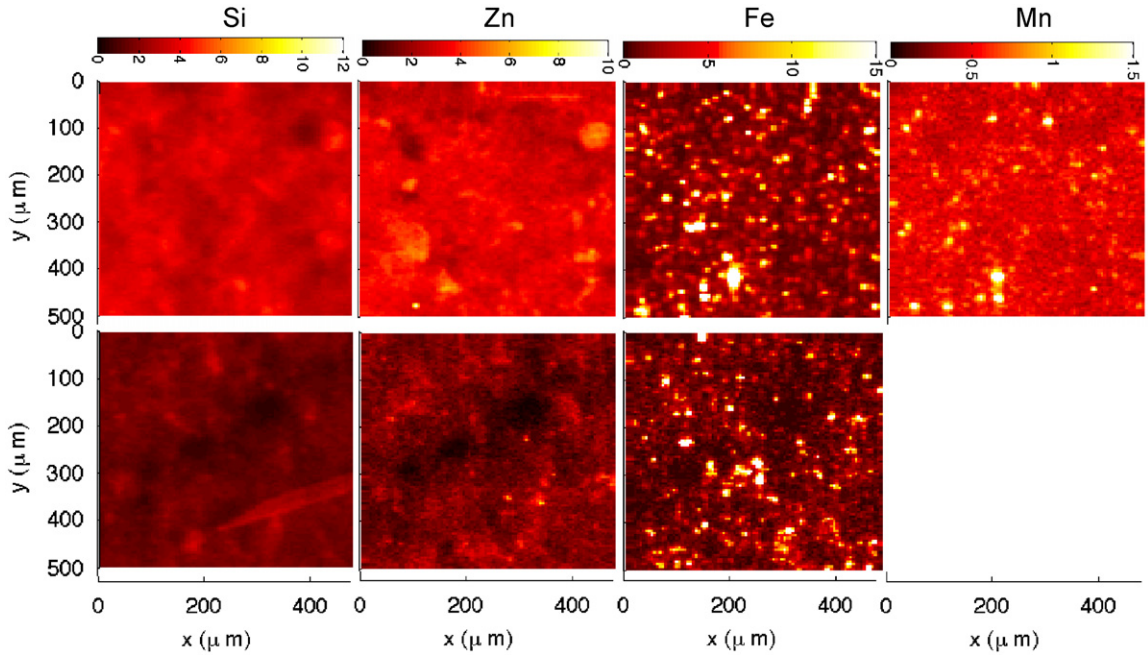

Fig. 7. Spatial distributions of Si, Zn, Fe and Mn in NBST trap samples from 300 m during the first deployment (first row) and second deployment (second row). Colorbars in units of pmol per pixel for Si, and fmol per pixel for Zn, Fe and Mn. Mn data not available for the second deployment. Each pixel is 5 μm.

Table 3
Summary of power law exponent values for non-linear fits of vertical flux data

Component	ALOHA "*b*"	K2 "*b*"
Al	0.51±0.29/−0.08±0.27	−0.92±0.21/−0.66±0.16
bSi	0.65±0.22/0.53±0.19	0.31±0.24/0.20±0.12
Co	−0.27±0.15/−0.73±0.82	0.57±0.97/−0.06±0.57
Cu	0.09±0.38/−0.32±0.25	0.00±0.40/−0.30±0.28
Fe	0.32±0.28/0.22±0.26	−1.11±0.20/−0.46±0.27
Mass	1.14±0.13/1.06±0.11	0.36±0.22/0.24±0.09
Mn	−0.62±0.63/−0.58±0.13	−1.27±0.27/−0.86±0.19
N	1.68±0.13/1.27±0.18	0.52±0.11/0.59±0.07
P	0.88±0.48/1.17±0.27	0.55±0.13/0.97±0.12
PIC	0.37±0.29/0.24±0.12	0.55±0.21/−0.04±0.21
POC	1.25±0.09/1.36±0.21	0.57±0.10/0.49±0.07
V	n/a	−0.05±0.12/−0.23±0.11
Zn	n/a	0.02±0.27/0.14±0.16

Only values for NBSTs are included. Values are first deployment/second deployment±1SE.

deeper depths in the ocean than the macronutricline (e.g., Johnson et al., 1997).

4.2.4. Trace element associations with biogenic material

Most of the elements reported here showed no correlation with particulate carbon (mostly organic carbon) fluxes at either site (Figs. 8 and 9). At K2, Fe and Mn exhibit a hint of increasing fluxes with decreasing C, but this is merely an artifact of increasing Fe and Mn inputs associated with the lateral plume and the attenuation of organic matter with depth. Zinc at K2 was the only trace element that showed a direct connection to the flux of biogenic material. The flux of Zn dropped substantially between deployments, in much the same way that POC and bSi did (Figs. 4 and 7). This is perhaps not surprising, as correlations between dissolved Zn and silicic acid in solution are well documented (e.g., Bruland et al., 1978), implying coupled biogeochemistry. Interestingly, the ratio of Zn to bSi in the trap material from K2 was about 5×10^{-4} (mole:mole; Fig. 10), which is comparable to the ratio observed in phytoplankton cells (ca. 2×10^{-4}; Twining et al., 2004) and in the solution phase for the NW Pacific (ca. 1×10^{-4}; Fujishima et al., 2001). The correlation is not strong within any one particular deployment, however, since the trend is suggested by the two groupings of points from the two deployments.

4.2.5. Micronutrient 1-D mass balance

Table 4 includes flux values estimated for several important biogeochemical processes that might affect the mesopelagic fluxes of Fe, Zn, Co and Cu, four micronutrient metals. A first-order flux balance model is a way to scale the important uptake and export fluxes of these micronutrients, and compare these terms to a single input source represented by dust at the top of the water column. We neglect lateral inputs for this exercise, which appears to be justified at ALOHA but is clearly a limitation at K2. The lateral inputs at K2 appeared to enhance particulate fluxes of Fe (and Al, Mn and Sc) at 300 and 500 m, but may not have impacted fluxes at 150 m very much during our sampling (more below). Furthermore, while lateral plume contributions of Fe to the euphotic zone have been suggested (e.g., Nishioka et al., 2007; Lam and Bishop, 2008), these are likely to occur during winter mixing and not be substantial during the summer stratified conditions during our occupation.

The dust inputs used were those by Measures et al. (2005), with Fe, Zn, Co and Cu values estimated by using the crustal averages of Wedepohl (1995). Uptake by autotrophs in the surface ocean is estimated by multiplying the primary production rates measured during the cruises (Boyd et al., 2008; Buesseler et al., 2008) by average cell quotas, estimated from several studies (e.g., Sunda et al., 1991; Sunda and Huntsman, 1992, 1995b; Ho et al., 2003; Twining et al., 2004; Finkel et al., 2006). It should be noted that by using cellular quota indices for the micronutrients, the "uptake" and flux of metals associated with biological material will be underestimated because extracellularly sorbed material has not been considered. A similar approach was used to estimate the export flux of the metals, by multiplying the cell quotas by the export/new production measured during the cruises (Elskens

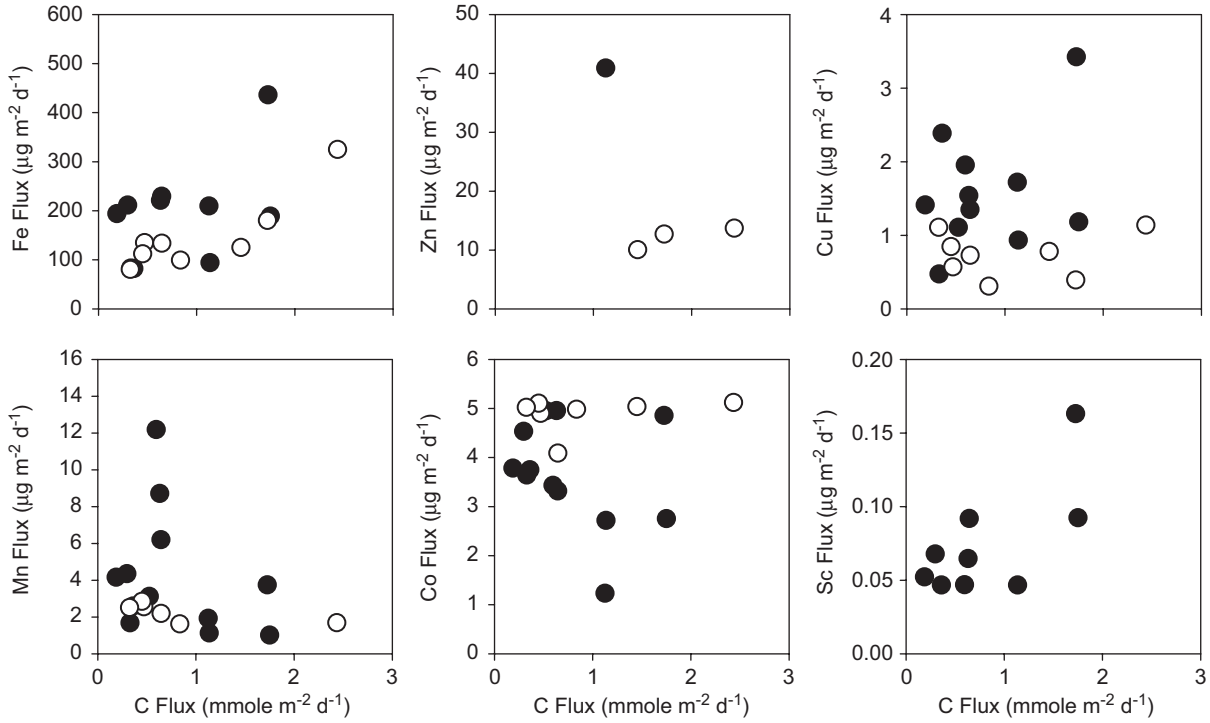

Fig. 8. Correlations of minor and trace element fluxes with C flux in sediment traps at ALOHA. NBST data only, with first deployment black and second in white.

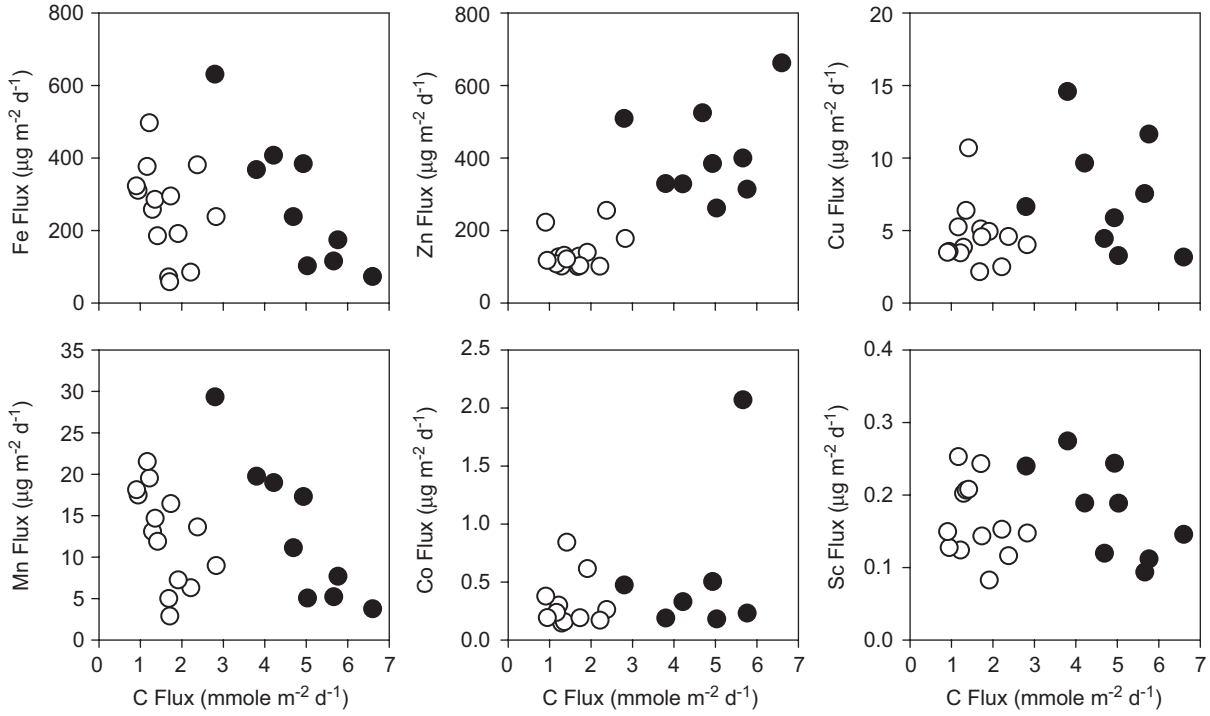

Fig. 9. Correlations of minor and trace element fluxes with C flux in sediment traps at K2. NBST data only, with first deployment black and second in white.

et al., 2008). These values are then compared to the sediment trap flux values. Not surprisingly, these four micronutrients appear to behave in very different ways from one another.

Iron dust fluxes balance those seen in the sediment traps fairly well (given the caveats discussed earlier), except below 150 m at K2, where lateral inputs are important (Table 4). The biological uptake appears to be a substantial fraction of the atmospheric input, but the export fluxes are very small by comparison. As has been frequently noted (e.g., Spokes et al., 1994; Jickells, 1999; Baker et al., 2006; Buck et al., 2006), a small percentage of the aerosol Fe input is "soluble" as determined by a variety of *in vitro* assays and therefore assumed to be bioavailable. These values

vary widely, but are frequently in the single digit percentage range. This is approximately the same percentage that export Fe flux represents of the total atmospheric input (Table 4). A comparable amount of dissolved Fe is also likely contributed to the euphotic zone at K2 following deep winter mixing of material supplied by a lateral plume (Nishioka et al., 2007). Thus, the 1-D model for Fe at both sites for 150 m and above suggests a system where much of the material falling through the water column is dust-derived with little accessed by organisms, which are instead drawing on a recycled pool of dissolved Fe in the euphotic zone and which appears to be sustainable by the "soluble" aerosol Fe flux as well as deep winter mixing at K2.

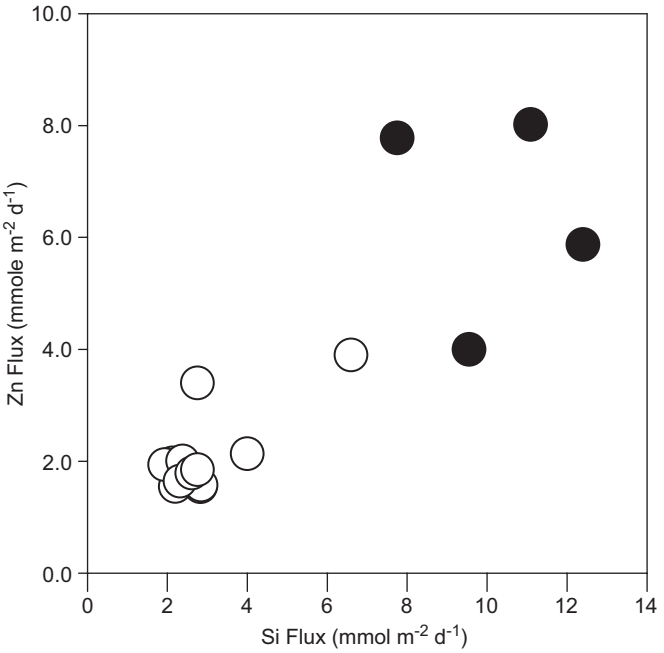

Fig. 10. Correlation of Zn flux with bSi flux in sediment traps from K2. NBST data only, with first deployment black and second in white.

The remineralization length scale of Fe (as reflected in the magnitude of their power law "b" values) observed during VERTIGO was substantially longer than POC. We must note, however, that the length scales for Fe estimated here are for total Fe found in the traps, which as noted in Table 4, is for a form of Fe that is present in large excess to that required by the producer community. Frew et al. (2006) found a similar trend when focusing on mostly biologically associated Fe in the much less dusty Southern Ocean during the FeCycle experiment.

A similar analysis for Zn is hampered somewhat by the lack of reliable trap data from ALOHA due to low fluxes, but a very different picture emerges nonetheless. For Zn at ALOHA, the atmospheric flux could possibly balance the export flux, representing a similar situation regarding soluble Fe dust inputs. However, this would require that 100% of aerosol inputs of Zn be available for biological uptake, which appears unlikely.

Rather, the situation at ALOHA may be more analogous to that at K2, where the atmospheric input appears inadequate to balance the export fluxes or the deeper fluxes. This would imply biological drawdown of a local/regional dissolved pool that is sustained through wintertime upwelling or much larger atmospheric inputs from anthropogenic sources, or some combination thereof. Lateral inputs of Zn to K2 are not indicated by vertical profiles of suspended particulates, unlike Fe and Mn (Bishop, pers. comm.). The vertical diffusion of Zn into the euphotic zone at K2 was estimated to be 3–30 $\mu g\,m^{-4}\,d^{-1}$ by using a dissolved Zn concentration gradient between 30 m (ca. 3 nM) and 70 m (ca. 5 nM) of ca. 3 $\mu g\,m^{-4}$ (Kinugasa et al., 2005) and vertical diffusivity of 1–10 $m^2\,d^{-1}$ (Talley et al., 1995). As noted recently by Croot et al. (2007) in estimating vertical diffusion of Fe, this approach is likely to be representative of a longer-term flux, and therefore probably an overestimate for summertime conditions. Therefore, the upward diffusional supply appears too slow to

Table 4
One-dimensional flux balances for four important micronutrients

Model term	Fe		Zn		Co		Cu	
	ALOHA	K2	ALOHA	K2	ALOHA	K2	ALOHA	K2
Dust and sediment trap fluxes								
Dust input[a]	15–92	36	0.019–0.115	0.053	7–40	20	0.02–0.09	0.021
150 m flux	208 ± 161	61/132	<60	408/162	<5000	209/96	1.8/0.75	6/4
300 m flux	170 ± 28	306/294	<60	390/116	<5000	261/198	1.5/0.58	9/5
500 m flux	134 ± 89	459/253	<60	372/139	<5000	355/409	1.7/1.3	6/6
Biological fluxes								
Cell quota[b]	5–10	0.6	0.2	4				
Bio. uptake	5–10	25/9	0.65	1.7/1.2	195	522/359	4	11/7
Export	0.6–1.2	2–6	0.08	0.2–0.4	25	117/66	0.5	2.4/1.3
Export/dust	0.65–8%	6–17%	70–421%	350%	63–360%	310%	>560%	>6200%
Pool and residence times								
Integrated pool[c]	2440 (2500)	840 (2500)	875	5900 (11,800)	190,000	88,350	4250	6350
Export residence time (d)	>2000	>140	>10,940	13,180	7600	755	8500	>2650
Flux residence time (d)	>12	>6	>15	>14	>38	>422	>2360	>1060

Units are $\mu g\,m^{-2}\,d^{-1}$, except for Co which is $ng\,m^{-2}\,d^{-1}$. Where available, uncertainties are included through use of the "±" sign. Alternatively, ranges are given where available. The columns for K2 often contain a forward slash, which is used to separate the estimates or measures for the first and second deployments. Biological uptake is calculated using the primary production estimates from the cruises (Boyd et al., 2008) and cellular metal quotas, while the shallow export is calculated with the new/export production estimates from the cruises (Elskens et al., 2008) and the same cellular quotas.

[a] Based on dust input estimates of Measures et al. (2005) and the crustal ratios of Wedepohl (1995).

[b] Cell quotas are in units of μmole Me:mole C; taken from Jickells et al. (1984); Knauer et al. (1984); Sunda et al. (1991); Sunda and Huntsman (1992, 1995a, b); Kuss and Kremling (1999); Ho et al. (2003); Pohl et al. (2004); Stanley et al. (2004); Twining et al. (2004); Finkel et al. (2006); Frew et al. (2006); Pohl et al. (2006).

[c] Units of the integrated pools are $\mu g\,m^{-2}$, except for Co, which is $ng\,m^{-2}$. This term calculated from dissolved concentrations (Bruland, 1980; Johnson et al., 1988; Lohan et al., 2002; Saito et al., 2003; Brown et al., 2005; Kinugasa et al., 2005; Noble et al., 2008), multiplied by the depth of the euphotic zone (125 m for ALOHA; 50 m for K2). Values in parentheses include particulate matter, if data are available (J.K.B. Bishop, pers. comm.).

sustain the overall downward flux (e.g., at 150 m), but may be more than adequate to balance the biology-driven export flux of Zn, implying some abiological Zn scavenging by sinking particles. If deep mixing/upwelling during winter is included with diffusion, all the Zn pool can be replenished (upwelling applied to deeper Zn concentration of 5 nM; winter upwelling rate of 0.043 m d^{-1}, Bograd et al., 1999), so that overall vertical supplies of Zn (convective and diffusive) can explain the cycling of Zn at K2.

The situation for Co is between that of Fe and Zn. The dust inputs are close to, but smaller than the mesopelagic fluxes, comparable to the export flux and much less than the biological uptake. Dust inputs appear important for Co, though perhaps inadequate to offset biological drawdown, which is supplemented by either a resupplied dissolved pool or additional non-crustal atmospheric inputs.

During our cruise to K2, primary production appeared to be Fe-limited (P. Boyd, pers. comm.), as has been observed in the past (e.g., Tsuda et al., 2003). The flux residence time (integrated pool divided by 150 m flux) is shorter for Zn than Co (Table 4), and it is much farther out of balance with atmospheric input than is Fe. This suggests that if no other Zn source were provided and if production were to persist at the rates observed, the system could conceivably switch from Fe to Zn limitation. However, an end to the growing season and deep winter mixing would likely occur before this switch-over.

The difference in flux of Co and Zn between the two sites is striking, with higher fluxes of Co at ALOHA and higher fluxes of Zn at K2. The dominant primary producers at ALOHA, cyanobacteria, have absolute requirements for Co for which Zn cannot substitute, and diatoms, the dominant producers at K2 appear to have higher Zn than Co requirements (e.g., Saito et al., 2002). Thus the between-site trend in Co and Zn fluxes is consistent with the requirements of their respective producer communities. However, the fluxes could be reflective of the relative abundance of these two metals at each site that are controlled by larger biogeochemical processes, with the producer community structure set, at least in part, by the concentrations.

Copper shows a very similar 1-D balance to that of Zn, with the atmospheric input appearing to be much smaller than either the biological uptake, export or mesopelagic flux. The export flux is of the same order, but appears slightly smaller than the mesopelagic flux, suggesting both biological uptake from a resupplied dissolved pool and sorption to sinking particles.

4.2.6. *Possible anthropogenic signals in the sinking flux (V and Zn at K2)*

At K2, sinking particles contained V concentrations that are slightly enriched relative to a crustal ratio with Al. However, if one views the V/Al ratio of the sinking particles as a function of depth (Fig. 11), the flux at 150 m is much more enriched in V relative to its crustal abundance, while deeper down, in the traps affected by the lateral input plume, the ratio approaches the crustal value. Furthermore, the enrichment is higher during the first deployment than during the second. Such a finding would suggest a scavenging type origin for V in sinking particle that is facilitated by biogenic material. Vanadium has been used as a tracer for oil burning in aerosols and therefore as a general anthropogenic tracer (e.g., Rahn and Lowenthal, 1984). A recent report (Sedwick et al., 2007) found that the V signal in aerosols collected over the Sargasso Sea was useful tracer of not only anthropogenic impact but also the solubility and potential bioavailability of Fe to that region. While these are very few data, the results could be explained through either a water column sorption mechanism (unlikely due to low V particle reactivity) or anthropogenic inputs. Non-mineral aerosols from Asia can be highly enriched in V, even

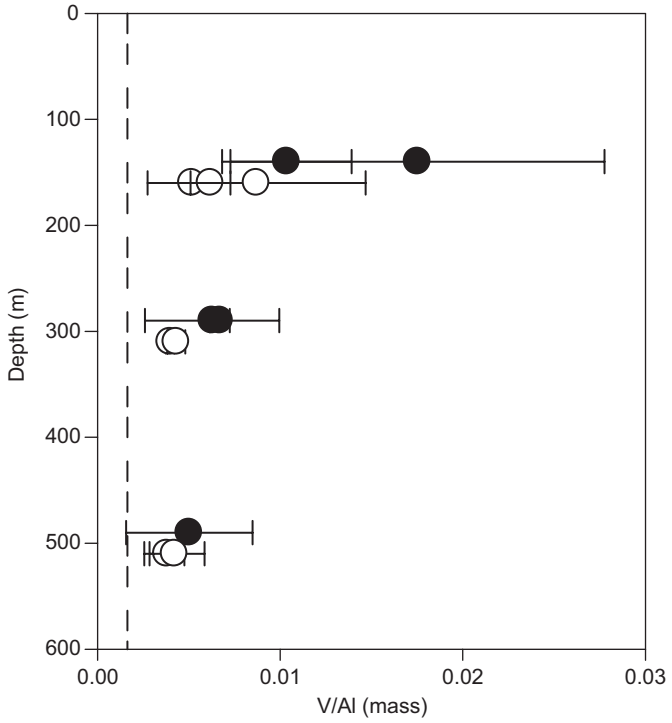

Fig. 11. V to Al ratio in sediment traps as a function of depth at K2. NBST data only, with first deployment black and second in white.

above those observed in our 150 m traps (Guo et al., 2004; Ma et al., 2004). The lack of a large enhancement in the two deeper trap depths suggests that the upper water column V could be swamped by the lateral plume signal, or that the V enrichment is somehow more soluble and lost from sinking particles during their transit of the mesopelagic zone.

In Section 4.2.5, we argued that atmospheric input of Zn at K2 (and probably at ALOHA) was inadequate to explain the flux out of the euphotic zone, and that organisms must therefore be sustained from a dissolved pool that is fed from other sources. An alternative explanation is that aerosols being deposited in the K2 region are highly enriched in Zn as a result of anthropogenic activities in Asia, providing an additional amount of this metal. As with V, there is data suggesting that atmospheric particles are greatly enriched in Zn above crustal values (100 ×) outside periods of the heavy spring dust loadings (e.g., Choi et al., 2001; Guo et al., 2004). This could mean that atmospheric Zn inputs were as much as 100 × fold higher than shown in Table 4, which could balance the estimated export flux of Zn, but not the total fluxes measured at 150 m or deeper. Without direct measurement of aerosols at K2, the impact of anthropogenic Zn on the system is impossible to confirm.

5. Conclusions

We have collected sinking particulate material from two very different oceanic systems and presented well-resolved flux profiles for a number of components, focusing in this report on minor and trace elements. The flux of trace and minor components were the result of a range of phenomena, including dust deposition and lateral inputs from continental shelves. The important micronutrient elements Fe, Zn and Co exhibited very different input and removal mechanisms, as well as a range of apparent biological availability/cycling (Fe the least to Zn the most). Lithogenic material did not follow trends exhibited by the

major/biogenic phases, suggesting significant decoupling for the removal of these particles from the rain of biological material from the surface.

Deep water trace element cycling, like that of POC, appears correlated to important sinking phases (e.g., Brewer et al., 1980; Martin and Knauer, 1983; Jickells et al., 1984; Armstrong et al., 2002). In the mesopelagic zone, however, we found little correlation between most metals and biogenic carrier material. Thus it would appear that important changes in the distribution and fate of trace elements occurs between the euphotic zone and more than 1000 m. Particle degradation, repackaging, dis- and reaggregation processes that are so frequently cited as important in determining the fate of organic carbon and macronutrients, are therefore probably important in determining the sorption/desorption and scavenging properties of marine particles.

Acknowledgments

Thanks to Chanda Bertrand, Jim Bishop, Phil Boyd, Frank Dehairs, Bill Fitzgerald, Makio Honda, Natalie Mahowald, Steve Manganini, Rob Mason, Steve Pike, Devin Ruddick, Dave Schneider and the captains and crews of the R/V *Kilo Moana* and *Roger Revelle*. Special thanks to Rod Johnson for supplying Sargasso Sea water and Rich Zuck for building the splitter. Thanks also to three reviewers for greatly improving the manuscript.

References

Andreev, A.G., Kusakabe, M., 2001. Interdecadal variability in dissolved oxygen in the intermediate water layer of the Western Subarctic Gyre and Kuril Basin (Okhotsk Sea). Geophysical Research Letters 28 (12), 2453–2456.

Antia, A.N., 2005. Particle-associated dissolved elemental fluxes: revising the stoichiometry of mixed layer export. Biogeosciences Discussions 2, 275–302.

Armstrong, R.A., Lee, C., Hedges, J.I., Honjo, S., Wakeham, S.G., 2002. A new, mechanistic model for organic carbon fluxes in the ocean based on the quantitative association of POC with ballast minerals. Deep-Sea Research II 49 (1–3), 219–236.

Baker, A.R., Jickells, T.D., Witt, M., Linge, K.L., 2006. Trends in the solubility of iron, aluminium, manganese and phosphorus in aerosol collected over the Atlantic Ocean. Marine Chemistry 98 (1), 43–58.

Bishop, J.K.B., Fleisher, M.Q., 1987. Particulate Manganese Dynamics in Gulf-Stream Warm-Core Rings and Surrounding Waters of the NW Atlantic. Geochimica et Cosmochimica Acta 51 (10), 2807–2825.

Bograd, S.J., Thomson, R.E., Rabinovich, A.B., LeBlond, P.H., 1999. Near-surface circulation of the northeast Pacific Ocean derived from WOCE-SVP satellite-tracked drifters. Deep-Sea Research II 46 (11–12), 2371–2403.

Boyd, P.W., Gall, M.P., Silver, M.W., Bishop, J.K.B., 2008. Quantifying the surface-subsurface biogeochemical coupling during the VERTIGO ALOHA and K2 studies. Deep-Sea Research II, this issue [doi:10.1016/j.dsr2.2008.04.010].

Brewer, P.G., Nozaki, Y., Spencer, D.W., Fleer, A.P., 1980. Sediment trap experiments in the deep North Atlantic: isotopic and elemental fluxes. Journal of Marine Research 38, 703–728.

Brown, M.T., Landing, W.M., Measures, C.I., 2005. Dissolved and particulate Fe in the western and central North Pacific: Results from the 2002 IOC cruise. Geochemistry Geophysics Geosystems 6 (10), 1–20.

Bruland, K.W., 1980. Oceanographic distributions of Cd, Zn, Cu and Ni in the North Pacific. Earth and Planetary Science Letters 47, 176–198.

Bruland, K.W., Knauer, G.A., Martin, J.H., 1978. Zinc in north-east Pacific waters. Nature 271, 741–743.

Buck, C.S., Landing, W.M., Resing, J.A., Lebon, G.T., 2006. Aerosol iron and aluminum solubility in the northwest Pacific Ocean: Results from the 2002 IOC cruise. Geochemistry Geophysics Geosystems 7 Art. No. Q04M07 APR 13 2006.

Buesseler, K.O., Steinberg, D.K., Michaels, A.F., Johnson, R.J., Andrews, J.E., Valdes, J.R., Price, J.F., 2000. A comparison of the quantity and composition of material caught in a neutrally buoyant versus surface-tethered sediment trap. Deep-Sea Research I 47 (2), 277–294.

Buesseler, K.O., Antia, A.N., Chen, M., Fowler, S.W., Gardner, W.D., Gustafsson, O., Harada, H., Michaels, A.F., Rutgers van der Loeff, M., Sarin, M., Steinberg, D.K., Trull, T., 2007a. An assessment of the use of sediment traps for estimating upper ocean particle fluxes. Journal of Marine Research 65, 345–416.

Buesseler, K.O., Lamborg, C.H., Boyd, P.W., Lam, P.J., Trull, T.W., Bidigare, R.R., Bishop, J.K.B., Casciotti, K.L., Dehairs, F., Elskens, M., Honda, M.C., Karl, D.M., Siegel, D., Silver, M.W., Steinberg, D.K., Valdes, J.R., Van Mooy, B., Wilson, S., 2007b. Revisiting carbon flux through the ocean's twilight zone. Science 316, 567–570.

Buesseler, K.O., Trull, T.W., Steinberg, D.K., Silver, M.W., Siegel, D.A., Saitoh, S.-I., Lamborg, C.H., Lam, P.J., Karl, D.M., Jiao, N.Z., Honda, M.C., Elskens, M., Dehairs, F., Brown, S.L., Boyd, P.W., Bishop, J.K.B., Bidigare, R.R., 2008. VERTIGO (VERtical Transport In the Global Ocean): a study of particle sources and flux attenuation in the North Pacific. Deep-Sea Research II, this issue [doi:10.1016/j.dsr2.2008.04.024].

Choi, J.C., Lee, M., Chun, Y., Kim, J., Oh, S., 2001. Chemical composition and source signature of spring aerosol in Seoul, Korea. Journal of Geophysical Research—Atmospheres 106 (D16), 18067–18074.

Collier, R., 1991. Analysis of particulate matter collected by sediment traps and from sediment cores. In: Hurd, D.C., Spencer, D.W. (Eds.), Geophysical Monograph 63. Marine Particles: Analysis and Characterization. American Geophysical Union, Washington, DC.

Croot, P.L., Frew, R.D., Sander, S., Hunter, K.A., Ellwood, M.J., Pickmere, S.E., Abraham, E.R., Law, C.S., Smith, M.J., Boyd, P.W., 2007. Physical mixing effects on iron biogeochemical cycling: FeCycle experiment. Journal of Geophysical Research—Oceans 112 (C6), Art. No. C06015 JUN 06020 02007.

Duce, R.A., Liss, P.S., Merrill, J.T., Atlas, E.L., Buat-Menard, P., Hicks, B.B., Miller, J.M., Prospero, J.M., Arimoto, R., Church, T.M., Ellis, W., Galloway, J.N., Hansen, L., Jickells, T.D., Knap, A.H., Reinhardt, K.H., Schneider, B., Soudine, A., Tokos, J.J., Tsunogai, S., Wollast, R., Zhou, M., 1991. The atmospheric input of trace species to the world ocean. Global Biogeochemical Cycles 5, 193–259.

Ducklow, H.W., Steinberg, D.K., Buesseler, K.O., 2001. Upper ocean carbon export and the biological pump. Oceanography 14 (4), 50–58.

Dymond, J., Lyle, M., 1985. Flux comparisons between sediments and sediment traps in the eastern tropical Pacific: implications for atmospheric CO_2 variations during the Pleistocene. Limnology and Oceanography 30, 69–712.

Elskens, M., Brion, N., Buesseler, K., Van Mooy, B.A.S., Boyd, P., Dehairs, F., Savoye, N., Baeyens, W., 2008. Primary, new and export production in the N.W. Pacific subarctic gyre during the VERTIGO K2 experiments. Deep-Sea Research II, this issue [doi:10.1016/j.dsr2.2008.04.013].

Finkel, Z.V., Quigg, A., Raven, J.A., Reinfelder, J.R., Schofield, O.E., Falkowski, P.G., 2006. Irradiance and the elemental stoichiometry of marine phytoplankton. Limnology and Oceanography 51 (6), 2690–2701.

Frankignoulle, M., Canon, C., Gattuso, J.P., 1994. Marine calcification as a source of carbon dioxide: positive feedback of increasing atmospheric CO_2. Limnology and Oceanography 39 (2), 458–462.

Frew, R.D., Hutchins, D.A., Nodder, S., Sanudo-Wilhelmy, S., Tovar-Sanchez, A., Leblanc, K., Hare, C.E., Boyd, P.W., 2006. Particulate iron dynamics during FeCycle in subantarctic waters southeast of New Zealand. Global Biogeochemical Cycles 20 (1), Art. No. GB1S93 MAR 98 2006.

Fujishima, Y., Ueda, K., Maruo, M., Nakayama, E., Tokutome, C., Hasegawa, H., Matsui, M., Sohrin, Y., 2001. Distribution of Trace Bioelements in the Subarctic North Pacific Ocean and the Bering Sea (the R/V *Hakuho Maru Cruise* KH-97-2). Journal of Oceanography 57 (3), 261–273.

Guo, Z.G., Feng, J.L., Fang, M., Chen, H.Y., Lau, K.H., 2004. The elemental and organic characteristics of PM2.5 in Asian dust episodes in Qingdao, China, 2002. Atmospheric Environment 38 (6), 909–919.

Ho, T.Y., Quigg, A., Finkel, Z.V., Milligan, A.J., Wyman, K., Falkowski, P.G., Morel, F.M.M., 2003. The elemental composition of some marine phytoplankton. Journal of Phycology 39 (6), 1145–1159.

Honda, M.C., Imai, K., Nojiri, Y., Hoshi, F., Sugawara, T., Kusakabe, M., 2002. The biological pump in the northwestern North Pacific based on fluxes and major components of particulate matter obtained by sediment-trap experiments (1997–2000). Deep-Sea Research II 49 (24-25), 5595–5625.

Huang, S., Sholkovitz, E.R., Conte, M.H., 2007. Application of high-temperature fusion for analysis of major and trace elements in marine sediment trap samples. L&O: Methods 5, 13–22.

Jickells, T.D., 1999. The inputs of dust derived elements to the Sargasso Sea: a synthesis. Marine Chemistry 68 (1–2), 5–14.

Jickells, T.D., Deuser, W.G., Knap, A.H., 1984. The sedimentation rates of trace elements in the Sargasso Sea measured by sediment trap. Deep-Sea Research 31 (10), 1169–1178.

Jickells, T.D., An, Z.S., Andersen, K.K., Baker, A.R., Bergametti, G., Brooks, N., Cao, J.J., Boyd, P.W., Duce, R.A., Hunter, K.A., Kawahata, H., Kubilay, N., laRoche, J., Liss, P.S., Mahowald, N., Prospero, J.M., Ridgwell, A.J., Tegen, I., Torres, R., 2005. Global iron connections between desert dust, ocean biogeochemistry, and climate. Science 308 (5718), 67–71.

Johnson, K.S., Stout, P.M., Berelson, W.M., Sakamoto-Arnold, C.M., 1988. Cobalt and copper distributions in the waters of Santa-Monica Basin, California. Nature 332 (6164), 527–530.

Johnson, K.S., Berelson, W.M., Coale, K.H., Coley, T.L., Elrod, V.A., Fairey, W.R., Iams, H.D., Kilgore, T.E., Nowicki, J.L., 1992. Manganese flux from continental-margin sediments in a transect through the oxygen minimum. Science 257 (5074), 1242–1245.

Johnson, K.S., Gordon, R.M., Coale, K.H., 1997. What controls dissolved iron concentrations in the world ocean? Marine Chemistry 57 (3–4), 137–161.

Karl, D.M., Michaels, A.F., 1996. The Hawaiian Ocean Time-series (HOT) and Bermuda Atlantic Time-series study (BATS). Deep-Sea Research II 43 (2-3), 127–128.

Kinugasa, M., Ishita, T., Sohrin, Y., Okamura, K., Takeda, S., Nishioka, J., Tsuda, A., 2005. Dynamics of trace metals during the subarctic Pacific iron experiment for ecosystem dynamics study (SEEDS2001). Progress in Oceanography 64 (2-4), 129–147.

Klaas, C., Archer, D.E., 2002. Association of sinking organic matter with various types of mineral ballast in the deep sea: implications for the rain ratio. Global Biogeochemical Cycles 16 (4), 1116–1129.

Knauer, G.A., Karl, D.M., Martin, J.H., Hunter, C.N., 1984. In situ effects of selected preservatives on total carbon, nitrogen and metals collected in sediment traps. Journal of Marine Research 42, 445–462.

Kremling, K., Streu, P., 1993. Saharan dust influenced trace-element fluxes in deep North-Atlantic subtropical waters. Deep-Sea Research I 40 (6), 1155–1168.

Kuss, J., Kremling, K., 1999. Particulate trace element fluxes in the deep northeast Atlantic Ocean. Deep-Sea Research I 46 (1), 149–169.

Lam, P.J., Bishop, J.K.B., 2008. The continental margin is a key source of iron to the HNLC North Pacific Ocean. Geophys. Res. Lett. 35 Art. No. L07608.

Lamborg, C.H., Buesseler, K.O., Valdes, J.R., Bertrand, C.H., Manganini, S., Pike, S., Steinberg, D., Trull, T., Wilson, S., 2008. The flux of bio- and lithogenic material associated with sinking particles in the mesopelagic "twilight zone" of the Northwest and North Central Pacific Ocean. Deep-Sea Research II, this issue [doi:10.1016/j.dsr2.2008.04.011].

Lee, C., Hedges, J.I., Wakeham, S.G., Zhu, N., 1992. Effectiveness of various treatments in retarding microbial activity in sediment trap material and their effects on the collection of swimmers. Limnology and Oceanography 37 (1), 117–130.

Lohan, M.C., Statham, P.J., Crawford, D.W., 2002. Total dissolved zinc in the upper water column of the subarctic North East Pacific. Deep-Sea Research II 49 (24–25), 5793–5808.

Ma, C.J., Tohno, S., Kasahara, M., Hayakawa, S., 2004. Properties of individual Asian dust storm particles collected at Kosan, Korea during ACE-Asia. Atmospheric Environment 38 (8), 1133–1143.

Mahowald, N.M., Baker, A.R., Bergametti, G., Brooks, N., Duce, R.A., Jickells, T.D., Kubilay, N., Prospero, J.M., Tegen, I., 2005. Atmospheric global dust cycle and iron inputs to the ocean. Global Biogeochemical Cycles 19 (4), Art. No. GB4025 DEC 4030 2005.

Martin, J.H., Knauer, G.A., 1983. VERTEX: manganese transport with $CaCO_3$. Deep-Sea Research 30, 411–426.

Martin, J.H., Knauer, G.A., Karl, D.M., Broenkow, W.W., 1987. VERTEX: carbon cycling in the NE Pacific. Deep-Sea Research 34, 267–285.

Measures, C.I., Vink, S., 2000. On the use of dissolved aluminum in surface waters to estimate dust deposition to the ocean. Global Biogeochemical Cycles 14 (1), 317–327.

Measures, C.I., Brown, M.T., Vink, S., 2005. Dust deposition to the surface waters of the western and central North Pacific inferred from surface water dissolved aluminum concentrations. Geochemistry Geophysics Geosystems 6 Art. No. Q09M03 SEP 13 2005.

Moffett, J.W., Ho, J., 1996. Oxidation of cobalt and manganese in seawater via a common microbially catalyzed pathway. Geochimica et Cosmochimica Acta 60 (18), 3415–3424.

Morel, F.M.M., Milligan, A.J., Saito, M.A., 2004. Marine bioinorganic chemistry: the role of trace metals in the oceanic cycles of major nutrients. H. Elderfield, Treatise on Geochemistry—Volume 6: The Oceans and Marine Geochemistry. Elsevier, Inc., San Diego, pp. 113–143.

Nameroff, T.J., Balistrieri, L.S., Murray, J.W., 2002. Suboxic trace metal geochemistry in the eastern tropical North Pacific. Geochimica et Cosmochimica Acta 66 (7), 1139–1158.

Nishioka, J., Ono, T., Saito, H., Nakatsuka, T., Takeda, S., Yoshimura, T., Suzuki, K., Kuma, K., Nakabayashi, S., Tsumune, D., Mitsudera, H., Johnson, W.K., Tsuda, A., 2007. Iron supply to the western subarctic Pacific: Importance of iron export from the Sea of Okhotsk. J. Geophys. Res.-Oceans 112 (C10), Art. No. C10012.

Noble, A.E., Saito, M.A., Maiti, K., Benitez-Nelson, C., 2008. Cobalt, manganese, and iron near the Hawaiian Islands: a potential concentrating mechanism for cobalt within a cyclonic eddy and implications for the hybrid-type trace metals. Deep-Sea Research II, in press [doi:10.1016/j.dsr2.2008.02.010].

Passow, U., De La Rocha, C.L., 2006. Accumulation of mineral ballast on organic aggregates. Global Biogeochemical Cycles 20 (GB1013, doi:10.1029/2005GB002579).

Pohl, C., Loffler, A., Hennings, U., 2004. A sediment trap flux study for trace metals under seasonal aspects in the stratified Baltic Sea (Gotland Basin; 57 degrees 19.20′N; 20 degrees 03.00′E). Marine Chemistry 84 (3-4), 143–160.

Pohl, C., Loffler, A., Schmidt, M., Seifert, T., 2006. A trace metal (Pb, Cd, Zn, Cu) balance for surface waters in the eastern Gotland Basin, Baltic Sea. Journal of Marine Systems 60 (3-4), 381–395.

Rahn, K.H., Lowenthal, D.H., 1984. Elemental tracers of distant regional pollution aerosols. Science 223, 132–139.

Reid, J.L., 1997. On the total geostrophic circulation of the pacific ocean: flow patterns, tracers, and transports. Progress in Oceanography 39 (4), 263–352.

Saito, M.A., Moffett, J.W., Chisholm, S.W., Waterbury, J.B., 2002. Cobalt limitation and uptake in *Prochlorococcus*. Limnology and Oceanography 47 (6), 1629–1636.

Saito, M.A., Moffett, J.W., DiTullio, G.R., 2003. Depletion of cobalt as a micronutrient in the eastern Equatorial Pacific. Geochimica et Cosmochimica Acta 67 (18), A409.

Sedwick, P.N., Sholkovitz, E.R., Church, T.M., 2007. Impact of anthropogenic combustion emissions on the fractional solubility of aerosol iron: Evidence from the Sargasso Sea. Geochem. Geophy. Geosy. 8, Art. No. Q10Q06.

Spokes, L.J., Jickells, T.D., Lim, B., 1994. Solubilization of aerosol trace-metals by cloud processing—a laboratory study. Geochimica et Cosmochimica Acta 58 (15), 3281–3287.

Stanley, R.H.R., Buesseler, K.O., Manganini, S.J., Steinberg, D.K., Valdes, J.R., 2004. A comparison of major and minor elemental fluxes collected in neutrally buoyant and surface-tethered sediment traps. Deep-Sea Research I 51, 1387–1395.

Steinberg, D.K., Cope, J.S., Wilson, S.E., Kobari, T., 2008. A comparison of mesopelagic zooplankton community structure in the subtropical and subarctic Pacific Ocean. Deep-Sea Research II, this issue [doi:10.1016/j.dsr2.2008.04.025].

Sunda, W.G., Huntsman, S.A., 1992. Feedback Interactions between Zinc and Phytoplankton in Seawater. Limnology and Oceanography 37 (1), 25–40.

Sunda, W.G., Huntsman, S.A., 1995a. Iron uptake and growth limitation in oceanic and coastal phytoplankton. Marine Chemistry 50 (1–4), 189–206.

Sunda, W.G., Huntsman, S.A., 1995b. Cobalt and zinc interreplacement in marine phytoplankton: biological and geochemical implications. Limnology and Oceanography 40 (8), 1404–1417.

Sunda, W.G., Swift, D.G., Huntsman, S.A., 1991. Low iron requirement for growth in oceanic phytoplankton. Nature 351 (6321), 55–57.

Talley, L.D., Nagata, Y., Fujimura, M., Iwao, T., Kono, T., Inagake, D., Hirai, M., Okuda, K., 1995. North Pacific intermediate water in the Kuroshio Oyashio mixed water region. Journal of Physical Oceanography 25 (4), 475–501.

Tsuda, A., Takeda, S., Saito, H., Nishioka, J., Nojiri, Y., Kudo, I., Kiyosawa, H., Shiomoto, A., Imai, K., Ono, T., Shimamoto, A., Tsumune, D., Yoshimura, T., Aono, T., Hinuma, A., Kinugasa, M., Suzuki, K., Sohrin, Y., Noiri, Y., Tani, H., Deguchi, Y., Tsurushima, N., Ogawa, H., Fukami, K., Kuma, K., Saino, T., 2003. A mesoscale iron enrichment in the western Subarctic Pacific induces a large centric diatom bloom. Science 300 (5621), 958–961.

Twining, B.S., Baines, S.B., Fisher, N.S., 2004. Element stoichiometries of individual plankton cells collected during the Southern Ocean Iron Experiment (SOFeX). Limnology and Oceanography 49 (6), 2115–2128.

Valdes, J.R., Price, J.F., 2000. A neutrally buoyant, upper ocean sediment trap. Journal of Atmospheric and Oceanic Technology 17 (1), 62–68.

Volk, T., Hoffert, M., 1985. Ocean carbon pumps: analysis of relative strengths and efficiencies in ocean-driven atmospheric CO_2 changes. In: Sundquist, E., Broecker, W.S. (Eds.), The Carbon Cycle and Atmospheric CO_2: Natural Variations Archean to Present. American Geophysical Union, Washington, DC, pp. 99–110.

Wedepohl, K.H., 1995. The composition of the continental crust. Geochimica et Cosmochimica Acta 59 (7), 1217–1232.

Zieman, J.J., Holmes, J.L., Connor, D., Jensen, C.R., Zoller, W.H., Hermann, D.M., Parrington, J.R., Gordon, G.E., 1995. Atmospheric aerosol trace element chemistry at Mauna Loa observatory.1. 1979–1985. Journal of Geophysical Research—Atmospheres 100 (D12), 25979–25994.